

Evaluation of water coning phenomenon in naturally fractured oil reservoirs

Reda Abdel Azim¹

Received: 13 September 2014 / Accepted: 17 May 2015 / Published online: 9 June 2015
© The Author(s) 2015. This article is published with open access at Springerlink.com

Abstract Water coning is a complex phenomenon observed in conventional and unconventional reservoirs. This phenomenon takes place due to the imbalance between viscous and gravitational forces during simultaneous production of oil and water. In a fractured reservoir, controlling of water coning is challenging due to the complexity originates from large number of uncertain variables associated with such reservoirs system. This paper presents a fully coupled poroelastic multiphase fluid-flow numerical model to provide a new insight and understanding of water coning phenomenon in naturally fractured reservoir under effect of various rock and fluid properties. These properties include anisotropy ratio, fracture permeability, mobility ratio, and production rate. The simulation workflow of the developed numerical model is based on upstream flux weighted finite element discretization method and a new hybrid methodology, which combines single-continuum and discrete fracture approach. Moreover, the capillary pressure effect is included during the discretization of the partial differential equations of multiphase fluid flow. The numerical system is decoupled using implicit pressure and explicit saturation (IMPES) approach. Discretization of water saturation equation using standard finite element method produces solution with spatial oscillations due to its hyperbolic nature. To overcome this, Galerkin's least square technique (GLS) is employed to stabilize the equation solutions. The developed numerical scheme is validated successfully against Eclipse-100 and then applied to a case study of fractured

reservoir taken from Southern Vietnam. The results showed that the break through time is very sensitive to the distributions of fracture network, anisotropy ratio between fracture horizontal, vertical permeability, and mobility ratio. Furthermore, it has been concluded that aquifer strength has a little effect on coning behavior during oil production process.

Keywords Water coning phenomenon · Naturally fractured reservoir · Finite element modelling

Introduction

Oil production from wells existing in reservoirs supported with a strong aquifer leads to changing of pressure draw-down around the wellbore and causing the movement of oil/water interface toward the producing interval. The fluid interface deforms from its initial shape into a cone shape and that is why this phenomenon is referred to coning (see Fig. 1). There are three essential forces controlling the mechanism of water coning which include capillary, gravity, and viscous forces. At initial reservoir conditions, the gravity force is dominant and once the wells start to flow the pressure drawdown increases and viscous force arises to be part of the controlling mechanisms (Hoyland et al. 1989). The oil/water interface moves up until viscous force is balanced with the gravitational force at a certain elevation. This balance can be achieved at a certain production flow rate and if such balance never occurred, the cone will be dragged up until invading the wellbore.

As a result of invading the wellbore by water cone, excessive water will be produced and kills the producing well or limiting its economic life (Beattie and Roberts 1996). The shape and the nature of the cone in conventional

✉ Reda Abdel Azim
eng_redarabee@hotmail.com

¹ School of Petroleum Engineering, The University of New South Wales, Sydney, NSW 2052, Australia

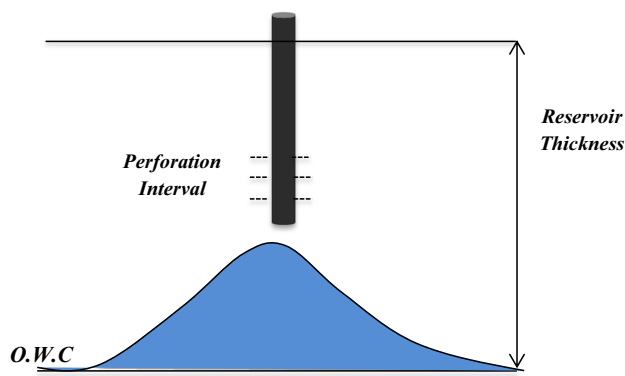


Fig. 1 A schematic representation explains the deformation of oil-water interface into a cone shape as result of oil production

reservoirs depend on numerous factors such as completion interval, production rate, anisotropy ratio, and mobility ratio (Inikori 2002). While, in naturally fractured reservoirs, the problem becomes more complicated due to the existence of two interacting porous media (fracture and matrix) which results in the formation of two cones. The first cone is the fastest and developed in fractures, while the slowest one is developed in the matrix porous media. The relative position of the two cones is rate sensitive and is a function of rock properties (Namani et al. 2007). If the well flows above the critical rate, the viscous force dominates and the cone will break into the wellbore. Therefore, the production flow rate plays a key role in limiting coning effects.

Hoyland et al. (1989) presented an analytical solution for critical flow rate calculations. The presented correlation is validated against numerical solutions. The authors concluded that the critical flow rate is independent on shape of water/oil relative permeability curve between endpoints, water viscosity, and wellbore radius, but it has a strong dependency on completion interval and permeability ratio k_v/k_h .

Al-Afaleg and Ershaghi (1993) used an empirical correlation for homogenous reservoirs to calculate the critical production rate and breakthrough time for naturally fractured reservoirs. Al Afaleg stated that no correlation or even simulation study has the capability to predict the estimation of critical production rate and breakthrough time if the fracture network is not accurately distributed.

Saad et al. (1995) performed an experimental work to assess the problem of water coning in naturally fractured reservoirs. The outcome of their experimental work was that the main factor influencing the breakthrough time is the difference in viscosities between oil and water phase. Furthermore, they stated that capillary forces may be neglected if the distance between oil water contact and fluid entry is sufficiently large compared to capillary rise.

Bahrami et al. (2004) assessed the coning phenomenon using actual water and gas coning data from Iranian natural

fractured reservoirs. By analyzing the results, it was concluded that the ratio k_v/k_h is the main factor controlling coning occurrence. Bahrami et al. (2004) presented a developed method suitable for calculation of breakthrough time and water cut at each specific oil production rate. They mentioned that the water invades the wellbore through fracture network and the breakthrough time is strongly dependant on fracture porosity. In addition, their study proved that the breakthrough time is very sensitive to horizontal and vertical fracture permeability. Perez-Martinez et al. (2012) evaluated the occurrence of coning in naturally fractured reservoirs using fine coning radial grid with one-meter thick layers concentric around the well and 2-inch thick layers in the annulus, with and without cement. They found that water coning takes place in fractured porous medium with permeability up to 10 Darcy's in both good and poorly cemented wells. Moreover, they developed a new correlation to determine maximum height of water coning, the breakthrough time, and well shut in time to reverse water cone.

Most of the previous studies simplify simulation of coning phenomenon by assuming that the dominant forces is only viscous force and capillary forces are therefore neglected. In the current study, the capillary forces are included during the derivation of the multiphase flow equations. The fluid production or injection alters the pressure state in fractured reservoirs that causes rock deformation and leads to generation of seismic activities. Moreover, the rock deformation leads to the change of porosity and permeability, which affects fluid flow, oil recovery, and coning phenomenon. To simulate these physical processes accurately, coupled effects need to be considered during simulation of mechanical and fluid-flow responses. For the above reasons, this study presents a new poroelastic numerical model to evaluate coning phenomenon in naturally fractured reservoirs. The model is for two-phase fluid flow through matrix and fractured medium. Furthermore, the model used a new hybrid methodology for fluid-flow simulation. In hybrid methodology, a threshold value for fracture length is defined. Fractures, which are smaller than the threshold value, are used to generate the grid-based permeability tensor. The reservoir domain is divided into a number of grid blocks, and the fluid-flow simulation is carried out using the single-continuum approach in the nominated blocks. Fractures, which are longer than the threshold value, are explicitly discretized in the domain using tetrahedral elements and the fluid-flow is modeled using the discrete fracture approach.

The model is validated against Eclipse-100 using horizontal fractures. In addition, the current paper presented a real case study of fractured reservoir taken from Southern Vietnam to evaluate parameters that affect water coning phenomenon.

Eclipse-100 is used as a dual porosity/permeability approach to simulate fluid flow in naturally fractured reservoirs. The dual porosity/permeability approach has a lot of limitations which include (1) the fluid distribution within the matrix blocks remains constant during the simulation period, (2) the model cannot be applied to disconnected and discrete fractured (oriented fractures) media and a small number of large scale fractures can be considered for flow simulation. Therefore, the developed numerical model that is presented in this paper overcomes all the abovementioned limitations by account flow through matrix porous media and discrete fractures by taking into account all fracture properties which include fracture orientation, radius, and location.

Methodology

Three-dimensional flow equations used for permeability tensor calculations are given by Darcy’s law and continuity equations as follows:

$$\begin{bmatrix} v_x \\ v_y \\ v_z \end{bmatrix} = - \begin{bmatrix} k_{xx} & k_{xy} & k_{xz} \\ k_{yx} & k_{yy} & k_{yz} \\ k_{zx} & k_{zy} & k_{zz} \end{bmatrix} \begin{bmatrix} \frac{\partial p}{\partial x} \\ \frac{\partial p}{\partial y} \\ \frac{\partial p}{\partial z} \end{bmatrix} = -\vec{k} \cdot \nabla p \tag{1}$$

$$\nabla \cdot v = 0, \tag{2}$$

where v is the fluid velocity vector, \vec{k} is the permeability tensor, and ∇p is the local pressure gradient. The grid-based permeability tensors for short to medium fractures are calculated using finite element technique. Each fracture is represented as a sandwiched element (triangular element) between three-dimensional tetrahedral elements representing the matrix porous media as shown in Fig. 2. Single-phase fluid-flow governing equation through matrix porous medium can be written as follows:

$$\nabla \cdot \left(\frac{\vec{k}}{\mu} \cdot \nabla p \right) + Q_H = 0. \tag{3}$$

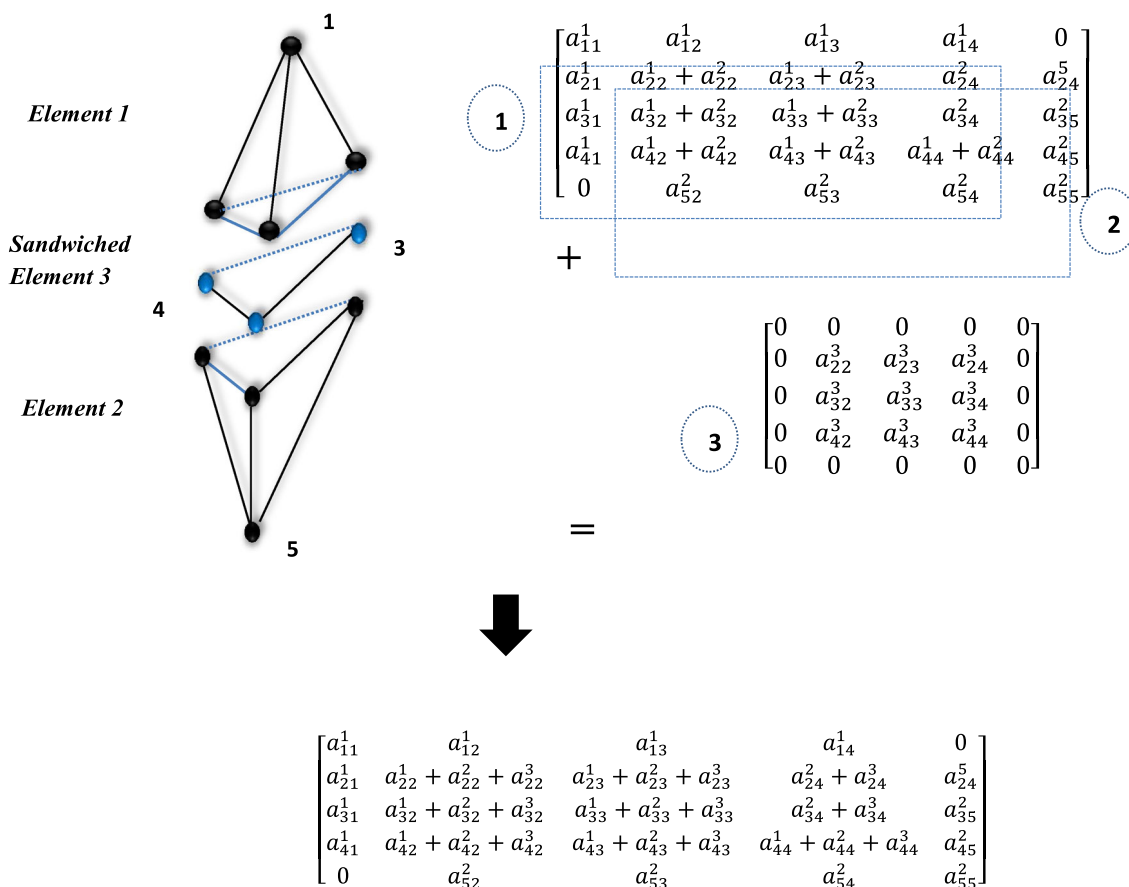


Fig. 2 Formulation of a full matrix in 3D space. Fracture is represented as (sandwich elements) and matrix elements (elements 1 and 2) assembled to be used during the simulation process

$$v = - \left(\frac{\vec{k}}{\mu} \cdot \nabla p \right), \tag{4}$$

where \vec{k} is a full permeability tensor, μ is the fluid viscosity, Q_H is fluid source/sink term represents the fluid exchange between matrix and fracture, or fluid extraction (injection) from the wellbore.

Single-phase fluid-flow governing equation through discrete fractures can be expressed as follows:

$$\nabla \left(\frac{k_f}{\mu} \cdot \nabla p_f \right) + q^+ + q^- = 0.0, \tag{5}$$

where q^+ and q^- are the leakage fluxes across the boundary interfaces, ∇ is the divergence operator in local coordinates system (Watanabe et al. 2010), and P_f is the pressure inside the fracture. The permeability of the fracture can be expressed by a parallel plate concept (cubic law) as shown in Eq. (6). It has been assumed that the fracture surfaces are parallel and the fluid-flow through a single discrete fracture is laminar (Snow 1969).

$$k_f = \frac{b^2}{12}, \tag{6}$$

where b is the fracture aperture, and k_f is the fracture permeability.

Finite element method formulation

The weighted residual method is used to derive the weak formulation of the governing equation of fluid flow through a fractured system. Standard Galerkin method is applied to discretize the weak forms with appropriate boundary conditions (Zimmerman and Bodvarsson 1996; Woodbury and Zhang 2001).

Equations (3) and (5) are written separately for matrix porous medium and discrete fractures in finite element formulation. The matrix is discretized using 3D tetrahedral elements and fractures are discretized using 2D triangle elements. If FEQ represents the flow equation, the integral form can be written as follows:

$$\iint_{\Omega} \text{FEQ} \, d\Omega = \int \int_{\Omega_m} \text{FEQ} \, d\Omega_m + b \times \int \int_{\Omega_f} \text{FEQ} \, d\bar{\Omega}_f, \tag{7}$$

where $\bar{\Omega}_f$ represents the fracture part of the domain as a 2D entity, Ω_m represents matrix domain, and Ω is the entire domain. 2D integral fracture equation is multiplied by the fracture aperture b for consistency of the integral form. The formulation of the governing equation for hydraulic process through matrix porous medium can be written as follows:

$$\nabla \left(\frac{\vec{k}}{\mu} \cdot \nabla p \right) + Q_H = 0.0. \tag{8}$$

Introducing weak formulation, Eq. (8) is expanded as follows:

$$\int_{\Omega} w \times \left(\begin{aligned} & \frac{\partial}{\partial x} \left(\frac{k_{xx} \partial p}{\mu \partial x} + \frac{k_{xy} \partial p}{\mu \partial y} + \frac{k_{xz} \partial p}{\mu \partial z} \right) \\ & + \frac{\partial}{\partial y} \left(\frac{k_{yx} \partial p}{\mu \partial x} + \frac{k_{yy} \partial p}{\mu \partial y} + \frac{k_{yz} \partial p}{\mu \partial z} \right) \\ & + \frac{\partial}{\partial z} \left(\frac{k_{zx} \partial p}{\mu \partial x} + \frac{k_{zy} \partial p}{\mu \partial y} + \frac{k_{zz} \partial p}{\mu \partial z} \right) \end{aligned} \right) + \int_{\Gamma} w^T q \, d\Gamma = 0, \tag{9}$$

where $[w = w(x, y, z)]$ is a trial function. The weak formulation for discrete fractures of Eq. (9) is expanded as follows:

$$\int_{\Omega_f} \nabla w \times \left(\frac{k_f}{\mu} \cdot \nabla p_f \right) + \int_{\Gamma_f} w \times q^+ \, d\Gamma + \int_{\Gamma_f} w \times q^- \, d\Gamma = 0.0. \tag{10}$$

Galerkin finite element method

Three basic steps in finite element approximation are (1) domain discretization by finite elements, (2) discretization of integral (weak) formulation, and (3) shape functions generation of field variables unknowns. Galerkin finite element method is used to discretize the integral weak forms of Eqs. (9) and (10). Unknown variables are approximated using appropriate shape functions.

$$p = N_p \times \bar{p}, \tag{11}$$

where N_p is the pressure shape function and \bar{p} is the vector of nodal values of the unknown variable. Finite element formulation of the governing equation for hydraulic process for matrix and fracture system can be written in a matrix form as follows:

$$\vec{M} \Delta \vec{p} = \vec{f} \tag{12}$$

$$\vec{M} = \vec{M}_f + \vec{M}_m \tag{13}$$

$$\vec{M} = \int_{\Omega} \nabla N_p^{mT} \frac{\vec{k}}{\mu} \nabla N_p^m \, d\Omega + \int_{\Gamma} \nabla N_p^{fT} \frac{k_f \times b}{\mu} \nabla N_p^f \, d\Gamma \tag{14}$$

$$\vec{f} = - \int_{\Gamma} N_p^{mT} Q_H \, d\Gamma - \vec{M}_f \times \bar{p}^{i-1^f} - \vec{M}_m \times \bar{p}^{i-1^m}, \tag{15}$$

where m is referring to matrix porous medium and f to fracture network.

Boundary conditions

Pressure and flux boundary conditions that have been presented by Durlafsky (1991) are used for calculations of permeability tensor in fractured porous medium. These conditions are listed in Eqs. (16)–(21) and Fig. 3.

$$p(y, x = 0, z) = p(y, x = 1, z) - G \quad \text{on } \partial D_3 \text{ and } \partial D_4 \quad (16)$$

$$u(y, x = 0, z) \cdot \vec{n}_3 = -u(y, x = 1, z) \cdot \vec{n}_4 \quad \text{on } \partial D_3 \text{ and } \partial D_4 \quad (17)$$

$$p(y = 0, x, z) = p(y = 1, x, z) - G \quad \text{on } \partial D_1 \text{ and } \partial D_2 \quad (18)$$

$$u(y = 0, x, z) \cdot \vec{n}_1 = -u(y = 1, x, z) \cdot \vec{n}_2 \quad \text{on } \partial D_1 \text{ and } \partial D_2 \quad (19)$$

$$p(y, x, z = 0) = p(y, x, z = 1) - G \quad \text{on } \partial D_5 \text{ and } \partial D_6 \quad (20)$$

$$u(y, x, z = 0) \cdot \vec{n}_5 = -u(y, x, z = 1) \cdot \vec{n}_6 \quad \text{on } \partial D_5 \text{ and } \partial D_6 \quad (21)$$

where n is the outward normal vector at the boundaries, ∂D is the grid block face, and G is the pressure gradient. Specifying a zero pressure gradient along the y -, z - faces ($\frac{\partial p}{\partial y} = 0$, and $\frac{\partial p}{\partial z} = 0$) and solving Eq. (12) with using the abovementioned periodic boundary conditions, the average velocity along x -, y -, and z - directions can be calculated as follows:

$$\langle v_x \rangle = - \int_{\partial D_3} v \cdot \vec{n}_3 dx dz \quad (22)$$

$$\langle v_y \rangle = - \int_{\partial D_1} v \cdot \vec{n}_1 dy dz \quad (23)$$

$$\langle v_z \rangle = - \int_{\partial D_5} v \cdot \vec{n}_5 dx dy \quad (24)$$

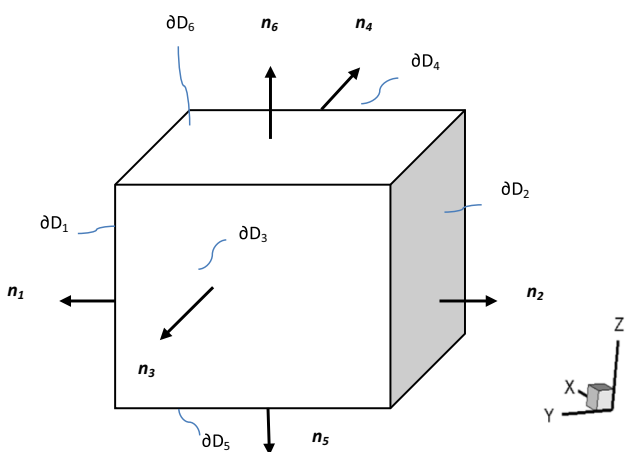


Fig. 3 Periodic boundary conditions used for over a grid block

Equation (1) can be expressed in an explicit form as follows:

$$v_x = -k_{xx} \frac{\partial p}{\partial x} - k_{xy} \frac{\partial p}{\partial y} - k_{xz} \frac{\partial p}{\partial z} \quad (25)$$

$$v_y = -k_{yx} \frac{\partial p}{\partial x} - k_{yy} \frac{\partial p}{\partial y} - k_{yz} \frac{\partial p}{\partial z} \quad (26)$$

$$v_z = -k_{zx} \frac{\partial p}{\partial x} - k_{zy} \frac{\partial p}{\partial y} - k_{zz} \frac{\partial p}{\partial z}, \quad (27)$$

where v_x , v_y , and v_z are velocities in x , y , and z directions, respectively. Since pressure gradient through x direction is assumed and v_x , v_y , and v_z are known, then k_{xx} , k_{xy} , and k_{xz} are easily determined. The rest of permeability tensor elements can be calculated using the same boundary conditions as abovementioned but in other directions.

Governing equations for multiphase poroelastic numerical model

In general, behavior of two-phase fluid-flow system through fractures network and matrix porous medium is controlled by generalized Darcy’s law and continuity equation of fluid flow for each fluid phase.

The Darcy’s law:

$$\phi s_\pi u^{\pi s} = \frac{k_{ij} k_{r\pi}}{\mu_\pi} [-p_\pi + \rho_\pi g_i] \pi = w, n_w \quad (28)$$

General continuity equation for wetting phase incorporating the concept of effective stress can be expressed as follows:

$$\begin{aligned} & - \nabla^T \left[\frac{k_{ij} k_{rw}}{\mu_w \beta_w} \nabla (p_w + \rho_w g h) \right] + \phi \frac{\partial}{\partial t} \left(\frac{\rho_w s_w}{\beta_w} \right) \\ & + \rho_w \frac{s_w}{\beta_w} \left[\left(1 - \frac{D}{3K_m} \right) \frac{\partial \varepsilon}{\partial t} + \frac{Dc}{3K_m} + \left(\frac{1 - \phi}{K_m} - \frac{D}{(3K_m)^2} \right) \frac{\partial \bar{p}}{\partial t} \right] + \rho_w Q_w = 0, \end{aligned} \quad (29)$$

General continuity equation for non-wetting phase can be expressed as follows:

$$\begin{aligned} & - \nabla^T \left[\frac{k_{ij} k_{ro}}{\mu_o \beta_o} \nabla (p_o + \rho_o g h) \right] + \phi \frac{\partial}{\partial t} \left(\frac{\rho_o s_o}{\beta_o} \right) \\ & + \rho_o \frac{s_o}{\beta_o} \left[\left(1 - \frac{D}{3K_m} \right) \frac{\partial \varepsilon}{\partial t} + \frac{Dc}{3K_m} + \left(\frac{1 - \phi}{K_m} - \frac{D}{(3K_m)^2} \right) \frac{\partial \bar{p}}{\partial t} \right] + \rho_o Q_o = 0, \end{aligned} \quad (30)$$

where ϕ is the porosity of the media, s_π is the saturation for each phase, $u^\pi s$ is the relative velocity vector between fluid phase and solid phase, k_{ij} is the permeability tensor, $k_{r\pi}$ is the relative permeability for each fluid phase π , μ_π , ρ_π , and p_π are dynamic viscosity, density of fluid, and fluid pressure for each phase, respectively, g_i is the gravity acceleration vector, β_π is the fluid formation volume factor, K_m is the bulk modulus of solid grain, D is the elastic stiffness matrix, and Q_π represents external sources or sinks.

Saturation equations

Oil saturation equation:

$$\phi \frac{\partial s_o}{\partial t} + \nabla v_o = 0.0 \tag{31}$$

Water saturation equation:

$$\phi \frac{\partial s_w}{\partial t} + \nabla v_w = 0, \tag{32}$$

where s_i and v_i are the saturation and velocity for phase i , respectively.

The discretization of these equations has been implemented using standard finite element method; also the partial differential equation used for calculating the saturation changes in fractures and matrix was discretized using Galerkin’s least square technique (GLS) to stabilize the equation solutions. To obtain the numerical solution of this highly nonlinear equations system, suitable initialization and boundary conditions should be designated at first, then some of auxiliary functions are employed which are known as the constitutive relationships.

Auxiliary equations

Saturation equation

The porous medium voids are assumed to be filled with water and oil and the sum of their saturation is unity:

$$s_o + s_w = 1. \tag{33}$$

The phase’s pressures in porous media are related through the capillary pressure equation as follows:

$$P_{cow} = P_o - P_w, \tag{34}$$

where p_{cow} is the capillary pressure between oil and water phase. The relative permeability coefficient of wetting and non-wetting phase depends on the degree of saturation and can be calculated either experimentally or using various relationships that have been proposed by different authors as shown in Table 1.

Table 1 Relative permeability function of two-phase fluid flow

Reference	Permeability function
Corey (1954)	$k_{rw} = s_e^4$ $k_{rmw} = (1 - s_e)^2 (1 - s_e^2)$
Brooks and Corey (1964)	$k_{rw} = s_e^{(2/\lambda)+3}$ $k_{rmw} = (1 - s_e)^2 (1 - s_e^{(2/\lambda)+1})$
Van Genuchten (1980)	$k_{rw} = \sqrt{s_e} (1 - (1 - s_e^{1/\gamma})^\gamma)^2$ $k_{rmw} = \sqrt{1 - s_e} (1 - s_e^{1/\gamma})^{2\gamma}$

s_e is the effective water phase saturation, and it equals to

$$s_e = \frac{s_w - s_{wr}}{s_{wmax} - s_{wr}}, \tag{35}$$

where s_{wr} is the residual water saturation, s_{wmax} is the maximum water saturation, λ is the pore size distribution index, and γ is an empirical constant to fit this relationship with the experimental data.

Finite element discretization

$$\begin{aligned} & - \int_{\Omega} \nabla N^T \frac{\rho_w k k_{rw}}{\mu_w \beta_w} \nabla N (p_w + \rho_w g h) dV \\ & + \int_{\Omega} N^T \phi s_w \frac{\rho_w}{K_w} \times N \frac{dp_w}{dt} dV + \int_{\Omega} N^T s_w \rho_w (1 - \phi) \\ & \times N \left\{ \frac{1 - \phi}{K_s} \times \left[s_w \frac{\partial p_w}{\partial t} - p_c \frac{\partial s_w}{\partial p_c} \left(\frac{\partial p_o}{\partial t} - \frac{\partial p_w}{\partial t} \right) + (1 - s_w) \frac{\partial p_o}{\partial t} \right] \right\} dV \\ & + N^T \phi \rho_w N \frac{\partial s_w}{\partial p_c} \left(\frac{\partial p_o}{\partial t} - \frac{\partial p_w}{\partial t} \right) dV - \int_{\Omega} N^T \frac{s_w \rho_w \phi}{s_w K_w + s_o K_o} \\ & \times N \left[-p_c \frac{\partial s_w}{\partial p_c} \left(\frac{\partial p_o}{\partial t} - \frac{\partial p_w}{\partial t} \right) + s_w \frac{\partial p_w}{\partial t} + (1 - s_w) \frac{\partial p_o}{\partial t} \right] dV \\ & + \int_{\Omega} N^T s_w \rho_w (1 - \phi) B \frac{\partial u}{\partial t} dV + Q = 0.0 \end{aligned} \tag{36}$$

Finite element method has been used to discretize two-phase fluid-flow governing equations in a poroelastic environment. where p_c is the capillary pressure, K_w is the water bulk modulus, and K_o is the oil bulk modulus. If FEQ represents the flow Eq. (36), the integral form for two-phase fluid flow through matrix and fracture can be written as follows:

$$\iint_{\Omega} \text{FEQ} d\Omega = \int \int_{\Omega_m} \text{FEQ} d\Omega_m + \int \int_{\Omega_f} \text{FEQ} d\bar{\Omega}_f,$$

where $\bar{\Omega}_f$ represents the fracture part of the domain as a 2D entity, Ω_m represents matrix domain, and Ω is the entire domain. The following flow chart explains how the developed numerical model works to simulate two-phase fluid flow in a poroelastic environment (see Fig. 4).

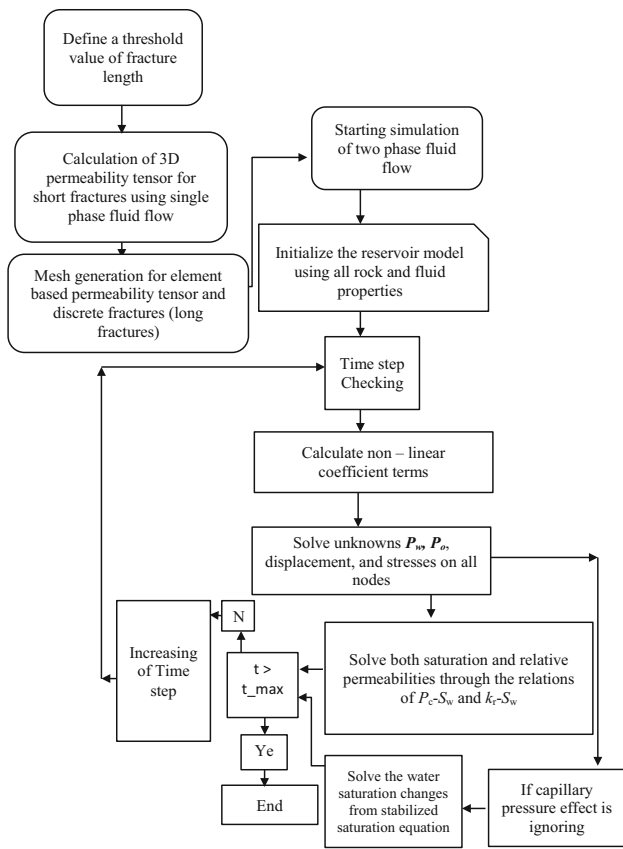


Fig. 4 Description of the computational procedure of two-phase fluid-flow calculations

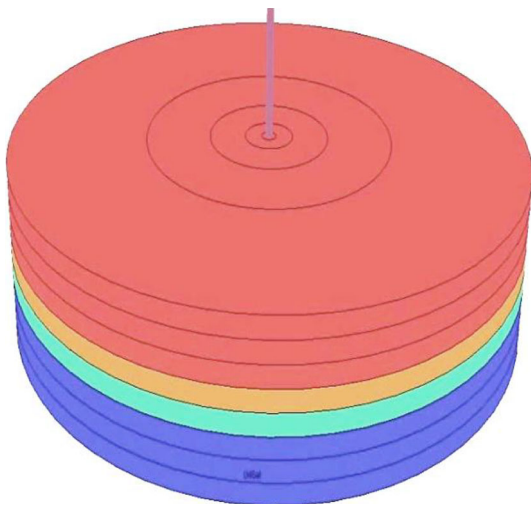


Fig. 5 Reservoir model used in Eclipse-100 with a set of horizontal fractures and a vertical well penetrating the model at layer 7 and 8

Validation of the developed numerical model

The performance of the developed 3D poroelastic numerical model is evaluated against Eclipse-100. A simple radial reservoir model consisting of 15 horizontal layers

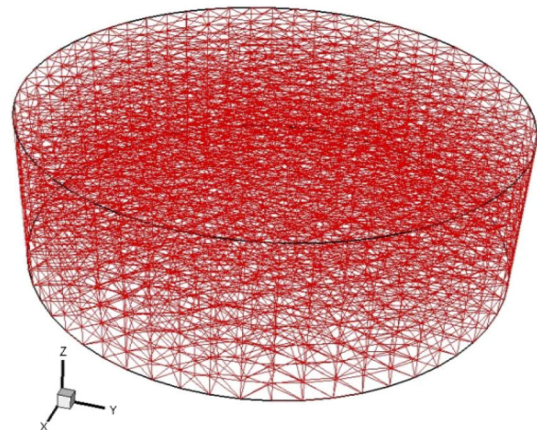


Fig. 6 Generated tetrahedral mesh with a set of horizontal fractures and a vertical well penetrating the model at layer 7 and 8

Table 2 Reservoir fluid properties used in the simulation of water coning

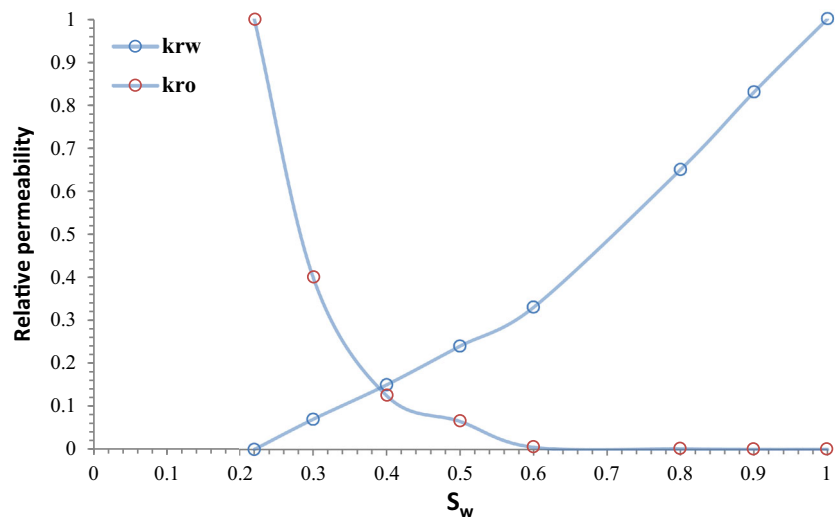
Water density (lbm/ft ³)	63.02
Water viscosity (cp)	0.96
Oil density (lbm/ft ³)	45.00
Oil viscosity (cp)	1.233
Formation volume factor (RB/STB)	1.0915

Table 3 Reservoir model properties used in the simulation of water coning

Reservoir thickness (ft)	100
Drainage radius (ft)	2098
Perforation interval (ft)	20
Well radius	0.20
Fracture porosity	0.001
Fracture permeability (md)	300
Matrix porosity	0.18
Matrix permeability (md)	1.25
Initial water saturation	0.22
Production rate (BPD)	3000

was built, eight layers represent the matrix porous medium, and the rest represents the fractures as shown in Fig. 5. Figure 6 shows the 3D generated mesh with the same physical dimensions of the reservoir model that has been created using Eclipse 100. A production well with radius of 0.2 ft is placed at the center of the model with producing interval in layer number 7 and 8. The rock and fluid properties used in this simulation model are extracted from Eclipse data files and presented in Tables 2 and 3. The same reservoir model has been studied with the developed poroelastic numerical model in this paper as well to prove its capability of modeling various real-field applications.

Fig. 7 Relative permeability curve used for fluid-flow simulation through matrix porous medium, $s_{wi} = 0.22$, $k_{ro}@s_{wi} = 0.98$ and $k_{rw}@s_{or} = 1.0$



The relative permeability curves used during the simulation process are presented in Figs. 7 and 8.

Simulation work

A base case run was performed under constant bottomhole pressure as a constraint to compare between Eclipse and developed numerical model results. Figure 9 shows oil production rate with time, while water cut at the production well is shown in Fig. 10.

As can be seen from Figs. 9 and 10, the oil production rate and water cut at the producer resulted from Eclipse-100 and the developed numerical simulation model is in agreement. Oil rate decreases with time, due to the increase of water rate production as a result of moving oil–water contact toward the producing interval. The model was simulated without the effect of stresses because the main aim was to validate the numerical model to be used in real-field applications. All fractures that used in this model are horizontal fractures where Eclipse 100 can handle.

Water flooding test in arbitrarily oriented fracture system

In example (1), water flooding is simulated in a single fracture (see Fig. 11a) and results of water saturation profile are presented in Fig. 11b. The reservoir dimensions are $10 \text{ m} \times 10 \text{ m} \times 4 \text{ m}$ in x , y , and z directions, respectively. The aperture of the fracture is assumed to be 0.15 mm and the matrix permeability is 2 md. Initial reservoir pressure is set at 3600 psi, one producer with constant bottomhole pressure set at 1500 psi, and the water injection rate is kept at 250 bbls/day. In example (2) same reservoir data are used, but the number of fractures is increased from one to

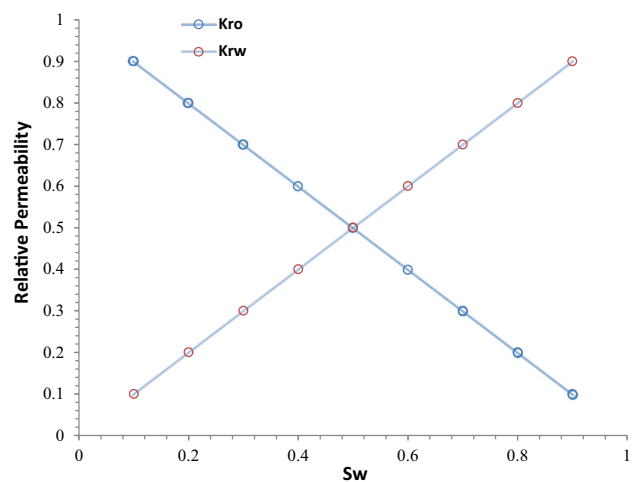


Fig. 8 Relative permeability curve used for fluid-flow simulation through discrete fractures

three (see Fig. 12a). In Fig. 12b, the water saturation profile after 1 h of water injection is presented. It can be seen from Figs. 11b and 12b that injected water displaced oil from the fractures first and then the matrix porous media.

Case study

The test case is taken from granitic oil-bearing formation in Southern offshore Vietnam. The formation is highly fractured and most of the fractures have short length identified from image logs and form the storage capacity of the reservoir. Geological interpretation showed that the reservoir has very low matrix porosity; permeability and pore spaces in the rock were formed through the fractures network and diagenetic processes. The authors used an innovative methodology to generate the 3D subsurface fracture map of the studied reservoir by integrating field data, such

Fig. 9 Eclipse 100 and developed numerical model results oil production rate vs time (base case) at constant bottomhole pressure (P_{wf}) = 3300 psi and reservoir pressure (P_r) = 3600 psi

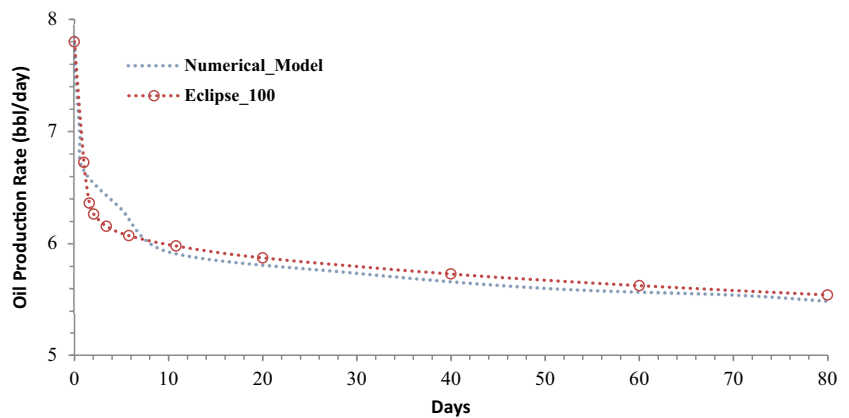


Fig. 10 Eclipse 100 and developed numerical model results for water cut vs time (base case) at constant bottomhole pressure (P_{wf}) = 3300 psi and reservoir pressure (P_r) = 3600 psi

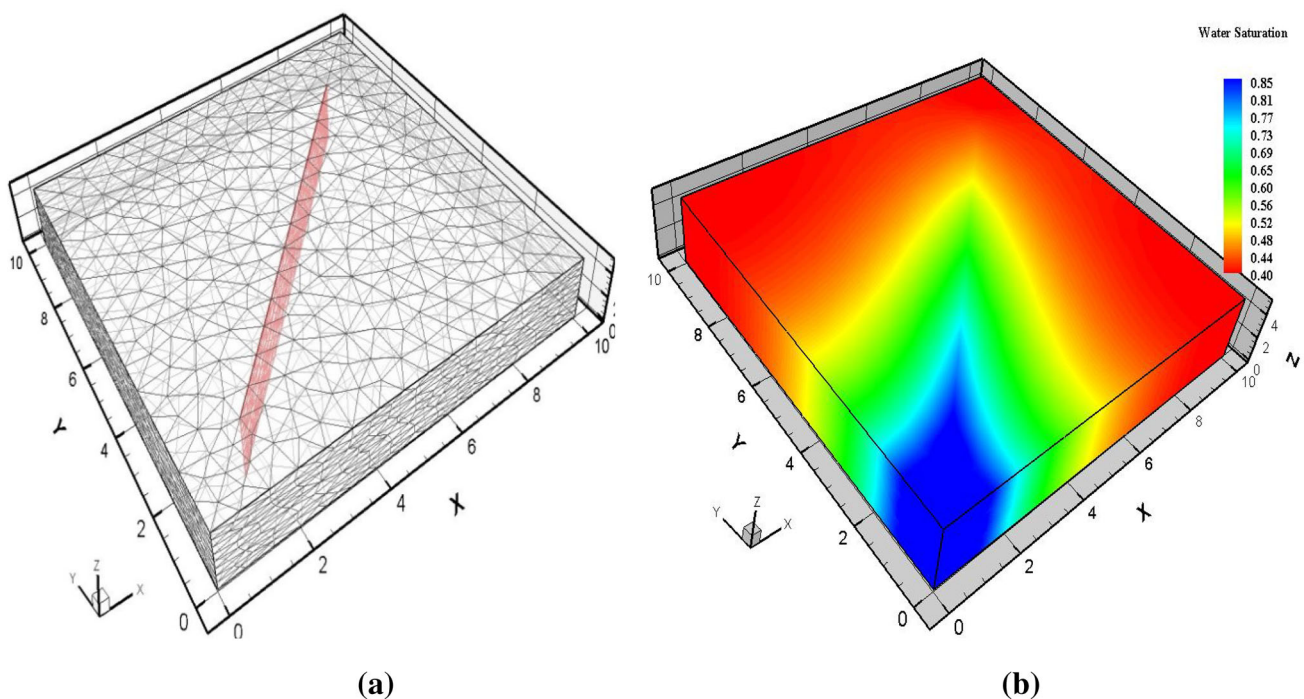
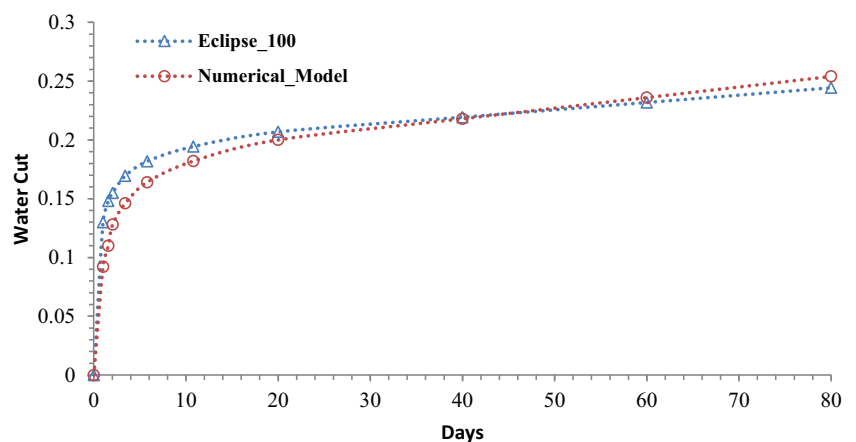


Fig. 11 Example (1): **a** Synthetic 3D fractured reservoir (10 m × 10 m × 4 m) studied in this example. The reservoir model containing one inclined fracture. The dip angle of the fracture is 90°

and azimuth angle is 315°. **b** Profiles of water saturation after 1 h of water injection (0.14 PV injected)

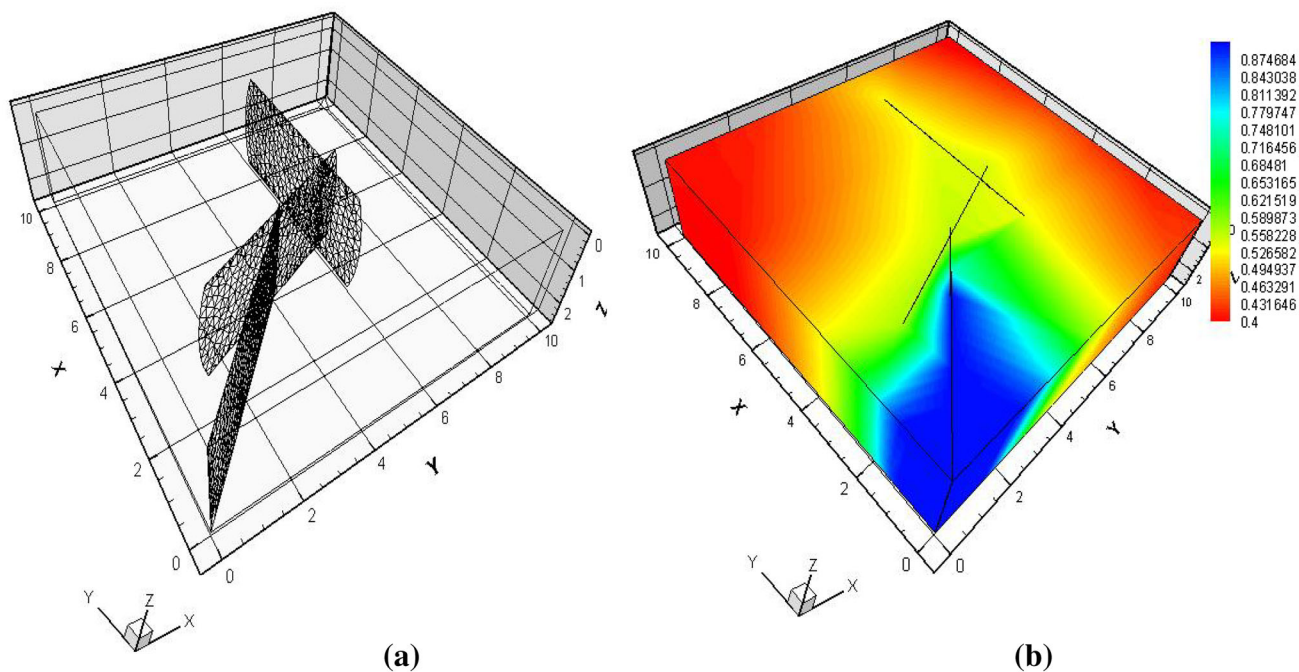


Fig. 12 Example (2): **a** Synthetic 3D fractured reservoir (10 m × 10 m × 2.5 m). The reservoir model contains three inclined fractures with dip angle 90° and azimuth angles are (315°, 337°, and 270°). **b** Profiles of water saturation after 1 h of water injection (0.125 PV injected)

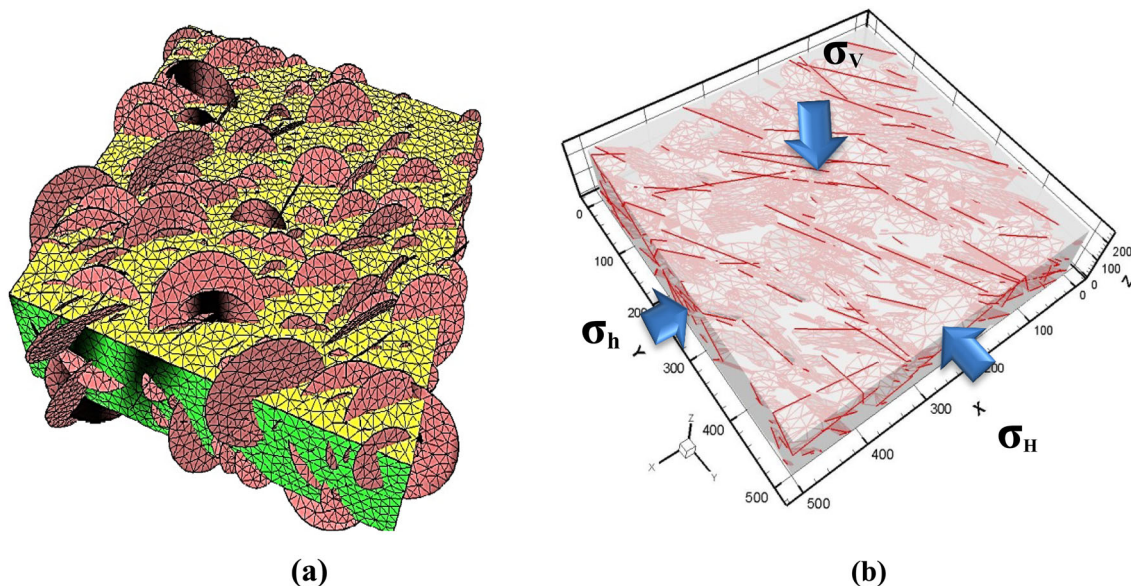


Fig. 13 **a** Generated subsurface fracture map using object-based model and **(b)** three dimensions mesh (tetrahedral elements for matrix and triangle elements for fractures) used in simulation process

as wellbore images and conventional well logs. In this approach, an object-based conditional global optimization technique is used to generate the subsurface fracture map

of the reservoir which combines statistical analysis of different sources of data as mentioned above (see Fig. 13a).

Generation of discrete fracture map of a typical basement reservoir

In this paper, object-based simulation technique is used to generate subsurface discrete fracture maps (Gholizadeh and Rahman 2012). In this model, fractures are treated as objects and placed in the domain stochastically. The number of generated fractures is controlled by fracture intensity and fractal dimension parameters. The fractures are treated as objects with varying radii, dips, and azimuth angles.

Study of water coning phenomenon

The coning phenomenon is studied using the generated fractured map (see Fig. 13a, b) under effect of different rock and fluid properties. Therefore, the model is initialized by applying vertical and horizontal stresses on *x*-, *y*-, and *z*-directions as shown in Fig. 13b. Because of the lack of information about far field stresses, the horizontal stresses are estimated based on overburden stress (Zoback 2010).

The fracture aperture is initialized using a value of 0.04 mm and its changes due to stresses effect are calculated using shear slippage criteria similar to Chen et al. (2000). Chen et al.’s (2000) criteria was based on the concept that when the pressure inside fracture becomes higher than the given in situ stress, the fracture opens and its surfaces no longer remain in contact. The oil–water contact is introduced to the model at depth = 250 m with 100 % water saturation and 0 % of oil saturation. Fluid and rock properties used in the simulation model are provided in Table 4. Relative permeability curves used for simulate fluid flow through matrix porous media and discrete fractures are presented in Fig. 14.

Table 4 Reservoir input data for Daihung fractured basement reservoir (Farak et al. 2009)

Parameter	Value
Reservoir dimensions	500 m × 500 m × 250 m
Matrix permeability	10 ⁻⁴ mD
Matrix porosity	2 %
Fracture aperture	0.04 mm
Initial fracture intensity	0.15 m ⁻¹
Fractal dimension (D)	1.25
Initial reservoir pressure	5063 psia
Fluid viscosity	1.38 cp
Fluid compressibility	10 ⁻⁵ psi ⁻¹
Horizontal stresses	4000 psi
Vertical stress	6800 psi

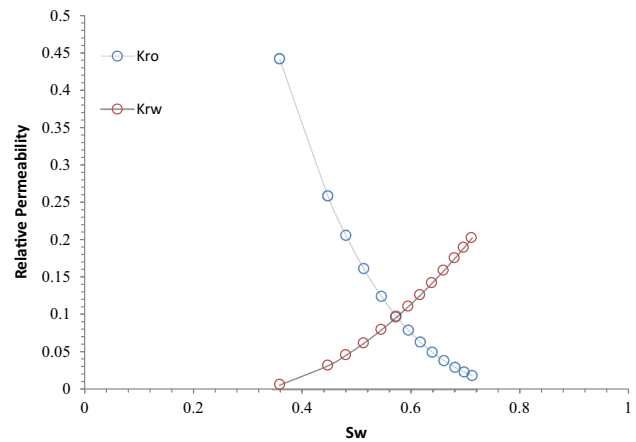


Fig. 14 Relative permeability curve used for fluid-flow simulation through matrix porous medium, $s_{wi} = 0.36$, $k_{ro}@s_{wi} = 0.45$ and $k_{rw}@s_{or} = 0.17$

Table 5 Anisotropy ratio values used in different simulation runs for evaluating coning phenomenon

Run	Anisotropy ratio k_v/k_h
1	2
2	1
3	0.6

The permeability tensors for short fractures with length smaller than 100 m are calculated using the method that has been described in the first part of the current paper. Fracture with length longer than 100 m is discretized explicitly in the domain using the triangular elements. The reservoir parameters that used for the sensitivity analysis are (1) anisotropy ratio k_v/k_h , (2) fracture permeability, and (3) oil production rate.

Anisotropy ratio k_v/k_h

First simulation runs are to evaluate the coning under effect of different anisotropy ratios k_v/k_h as shown in Table 5.

Figure 15 shows the effect of anisotropy ratio on water cut. The result indicates that the water cut increases as a result of increasing the anisotropy ratio value. The physical explanation behind that is the increase of vertical permeability will enhance the coning into the fractured network due to the pressure drawdown around the wellbore.

Oil production rate

Figure 16 shows the effect of changing oil production rate on the producing water cur. As can be seen from this figure (Fig. 16), decrease in oil production rate delays the water breakthrough time significantly.

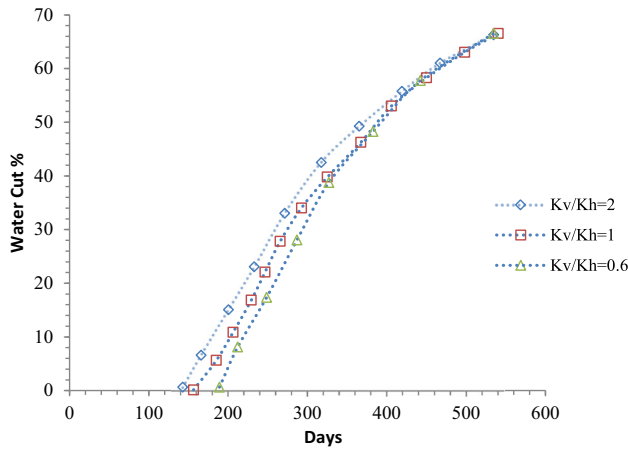


Fig. 15 Effect of anisotropy ratio on produced water cut with $P_{init} = 5063$ psi, $\sigma_H = 4000$ psi, $\sigma_h = 4000$ psi, and $\sigma_v = 6800$ psi

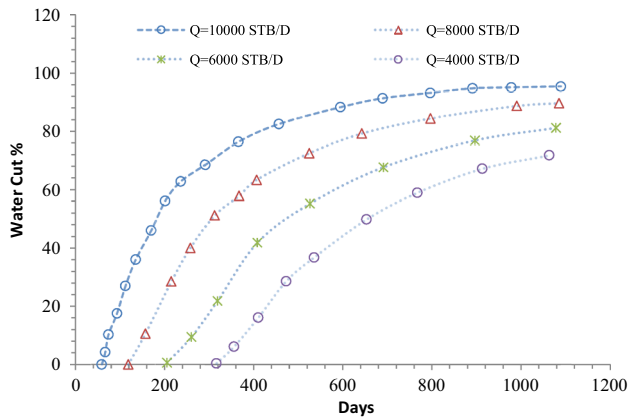


Fig. 16 Effect of oil production rate on produced water cut with $P_{init} = 5063$ psi, $\sigma_H = 4000$ psi, $\sigma_h = 4000$ psi, and $\sigma_v = 6800$ psi

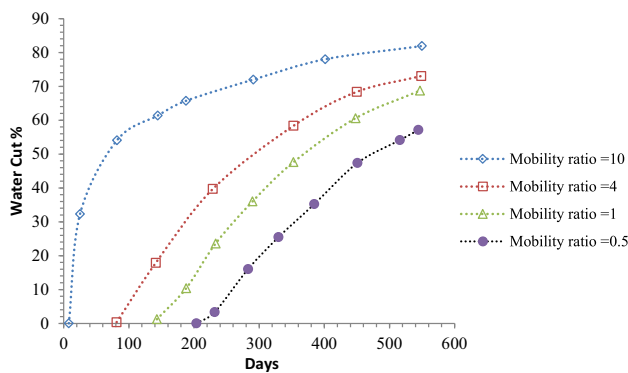


Fig. 17 Effect of mobility ratio on produced water cut with $P_{init} = 5063$ psi, $\sigma_H = 4000$ psi, $\sigma_h = 4000$ psi, and $\sigma_v = 6800$ psi

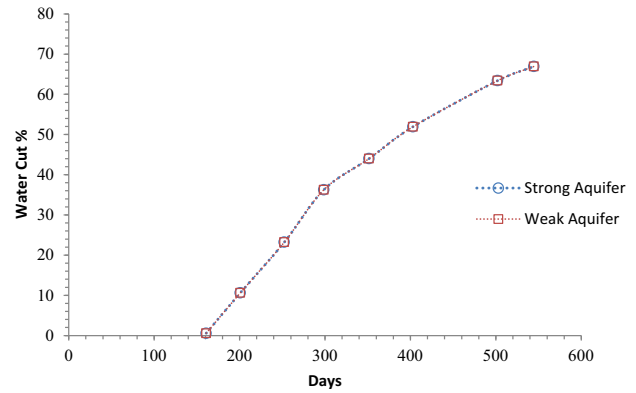


Fig. 18 Effect of aquifer strength on produced water cut with $P_{init} = 5063$ psi, $\sigma_H = 4000$ psi, $\sigma_h = 4000$ psi, and $\sigma_v = 6800$ psi

Mobility ratio

Four mobility ratios are selected to perform the sensitivity analysis as shown in Fig. 17. As expected at high mobility ratio ($\mu = 10$), the breakthrough time occurs very fast (5.5 days). On the other hand, when mobility ratio becomes very small ($\mu = 0.5$), the breakthrough time occurs after 200 days of oil production.

Aquifer strength

One strong aquifer and weak aquifer are tested in the fractured reservoir model. Simulation results in Fig. 18 show that the aquifer characteristics have no effect on the breakthrough time and the water cut after breakthrough.

Conclusion

A 3D multiphase poroelastic numerical model is developed to assess the water coning phenomenon in naturally fractured reservoirs. The developed numerical model has the ability to simulate large numbers of discrete fracture in the reservoir domain. Several parameters have been used to assess their effects and contribution to the water coning phenomenon in naturally fractured reservoirs. These parameters are anisotropy ratio, mobility ratio, oil production, and the aquifer strength.

The conclusion that can be drawn from the simulation study are as follows:.

- Increase in the vertical permeability [i.e., increase in anisotropy ratio (k_v/k_h)] leads to increase of water cut

and water saturation at the producing interval without any significant effect on the oil production rate from the fractured reservoir.

- Decrease of oil production rate leads to decrease of produced water cut. The physics explanation is to the fact that at low rate, water cut is controlled by fast moving cone inside the fractures.
- Aquifer strength has a little effect on produced water cut.
- Investigation of the effective parameters is necessary to understand the mechanism of water coning in naturally fractured reservoirs. Simulation of this phenomenon helps to optimize the conditions in which the breakthrough time of water cone is delayed.

Open Access This article is distributed under the terms of the Creative Commons Attribution 4.0 International License (<http://creativecommons.org/licenses/by/4.0/>), which permits unrestricted use, distribution, and reproduction in any medium, provided you give appropriate credit to the original author(s) and the source, provide a link to the Creative Commons license, and indicate if changes were made.

References

- Al-Afaleg NI, Ershaghi I (1993) Coning phenomena in naturally fractured reservoirs. Society of Petroleum Engineers Paper, SPE 26083
- Bahrami H, Shadzadeh SR, Goodarzniya I (2004) Numerical simulation of coning phenomena in naturally fractured reservoirs. Paper presented at the 9th Iranian Chemical of Engineering Congress (IchEC9), Iran University of Science and Technology (IUST), 23–25 November
- Beattie DR, Roberts BE (1996) Water coning in naturally fractured gas reservoirs. Society of Petroleum Engineers Paper, SPE 35643
- Brooks RH, Corey AT (1964) Hydraulic properties of porous media. Colorado State University Hydrology Paper 3. State University, Fort Collins, CO
- Chen Z, Narayan SP, Yang Z, Rahman SS (2000) An experimental investigation of hydraulic behaviour of fractures and joints in granitic rock. *Int J Rock Mech Min Sci* 37:1061–1071
- Corey AT (1954) Interrelation of gas and oil relative permeabilities. *Prod Mon* 19(1):38–41
- Durlofsky LJ (1991) Numerical calculation of equivalent grid block permeability tensors for heterogeneous porous media. *Water resour res* 27(5):699–708
- Farag SM, Le HV, Mas C, Maizeret P-D, Li B, Dang T (2009) Advances in granitic basement reservoir evaluation. Society of Petroleum Engineers. doi:10.2118/123455-MS
- Gholizadeh DN, Rahman SS (2012) 3D hybrid tectono-stochastic modeling of naturally fractured reservoir: Application of finite element method and stochastic simulation technique. *Tectonophysics* 541–543(0):43–56
- Hoyland AL, Papatzacos P, Skjæveland MS (1989) Critical Rate for water coning: correlation and analytical solution. Society of Petroleum Engineers Paper, SPE 15855
- Inikori SO (2002) Numerical study of water coning control with downhole water sink (DWS) well completions in vertical and horizontal wells. The Department of Petroleum Engineering, Louisiana State University. Doctor of Philosophy, p 238
- Namani M, Asadollahi M, Haghghi M (2007) Investigation of water coning phenomenon in Iranian carbonate fractured reservoirs. Society of Petroleum
- Perez-Martinez E, Rodriguez-de la Garza F, Samaniego-Verduzco F (2012) Water coning in naturally fractured carbonate heavy oil reservoir—a simulation study. Society of Petroleum Engineers Paper, SPE 152545
- Saad SM, Darwich TD, Asaad Y (1995) Water coning in fractured basement reservoirs. Society of Petroleum Engineers Paper, SPE 29808
- Snow DT (1969) Anisotropic permeability of fractured media. *Water Resour Res* 5(6):1273–1289
- Van Genuchten MTH (1980) A closed form equation for predicting the hydraulic conductivity of unsaturated soils. *Soil Sci Soc Am J* 44(5):892–898
- Watanabe N, Wang W, McDermott CI, Taniguchi T, Kolditz O (2010) Uncertainty analysis of thermo-hydro-mechanical coupled processes in heterogeneous porous media. *Comput Mech* 45(4):263–280
- Woodbury A, Zhang K (2001) Lanczos method for the solution of groundwater flow in discretely fractured porous media. *Adv Water Resour* 24(6):621–630
- Zimmerman RW, Bodvarsson GS (1996) Hydraulic conductivity of rock fractures. *Transp porous media* 23(1):1–30
- Zoback MD (2010) Reservoir geomechanics. Cambridge University Press, Cambridge